Nanoelectronics and Its New Materials – A NEW ERA OF NANOSCIENCE

Nanoelectronics and Its New Materials –
A NEW ERA OF NANOSCIENCE

ZEISS
Seeing beyond

WILEY

Discover the recent advances in electronics research and fundamental nanoscience.

Nanotechnology has become the driving force behind breakthroughs in engineering, materials science, physics, chemistry, and biological sciences. In this compendium, we delve into a wide range of novel applications that highlight recent advances in electronics research and fundamental nanoscience. From surface analysis and defect detection to tailored optical functionality and transparent nanowire electrodes, this eBook covers key topics that will revolutionize the future of electronics.

To get your hands on this valuable resource and unleash the power of nanotechnology, simply download the eBook now. Stay ahead of the curve and embrace the future of electronics with nanoscience as your guide.

ZEISS

Seeing beyond

WILEY

Configurationally Confined Multilevel Supramolecular Assemblies for Modulating Multicolor Luminescence

Mengdi Tian, Ze Wang, Xing Yuan, Heng Zhang,* Zhixue Liu,* and Yu Liu*

Herein, multilevel supramolecular assemblies are reported based on sulfobutylether-β-cyclodextrin (SBE-βCD) and cucurbit[8]uril (CB[8]), which can control the topological morphology from nanoparticles to nanosheets and modulate the multicolor luminescence. Benefiting from the large cavity of CB[8] and its strong binding affinity with positively charged tetraphenylethylene pyridinium (TPE-Py), a 1:2 stoichiometric supramolecular assembly is formed through host–guest interactions with binding constants of 2.95×10^{11} M^{-2} and fluorescence bathochromic shift about 35 nm due to the macrocyclic confinement effect, thereby endowing the fluorescence enhancement about 20 times when further assembled with negatively charged SBE-βCD to form nanosheets through electrostatic interactions. In contrast, the direct assembly of TPE-Py and SBE-βCD can form nanoparticles through electrostatic interactions, showing only tenfold enhancement and no bathochromic shift due to the lack of macrocyclic confinement effect. After doping the near-infrared dye acceptor sulfonated aluminum phthalocyanine (AlPcS4), the nanosheets structure exhibits a higher energy transfer efficiency of about 75% and a larger antenna effect of 29.3 than that of nanoparticles. The multilevel supramolecular assemblies can be used in multicolor luminescence information storage and multiple logical gate systems, providing an efficient approach for configurationally confined topological morphology regulation and luminescent materials.

1. Introduction

Taking advantage of noncovalent interactions to construct multilevel supramolecular assemblies is one of the hot topics in supramolecular research. By means of the multiple hydrogen bonds,[1] halogen bonds,[2] macrocycles encapsulation interactions,[3] metal coordination interactions,[4] noncovalent polymerization,[5] the formed supramolecular assemblies have been widely used in the luminescent materials,[6] energy transfer,[7] molecular recognition,[8] hydrogels,[9] and information security.[10] Therefore, many researches have been reported on the multilevel supramolecular assemblies. Among them, macrocycle primary confinement and assembly secondly confinement are very important strategies because they can modulate the photophysical behaviors of assembly by changing the topological morphology. For example, George and co-workers reported that cationic phthalimide derivative can be encapsulated by cucurbit[7]uril (CB[7]) or assembled with laponite clays through the electrostatic interactions, achieving efficient room-temperature phosphorescence, which can be served as light-harvesting energy transfer platform for fluorescent dyes.[11] Our group reported noncovalent polymerization-activated long-lived near-infrared fluorescent assemblies based on CB[7]/β-cyclodextrin confined purely organic room-temperature phosphorescence harvesting system for lysosome-targeted imaging.[12] In particular, two macrocycles such as cucurbit[8]uril (CB[8]) and negatively charged calixarene, were coassembled with organic dyes, giving the topological morphology changes from nanorods to nanoparticles, which not only redshifted the emission of dyes, but also enhanced their fluorescence intensity.[13] It can be seen that by using two or more kinds of noncovalent interactions is conducive to the construction of multilevel supramolecular assemblies. However, there are few reports on the research of changing the topological morphology to modulate the Förster resonance energy transfer (FRET) process.
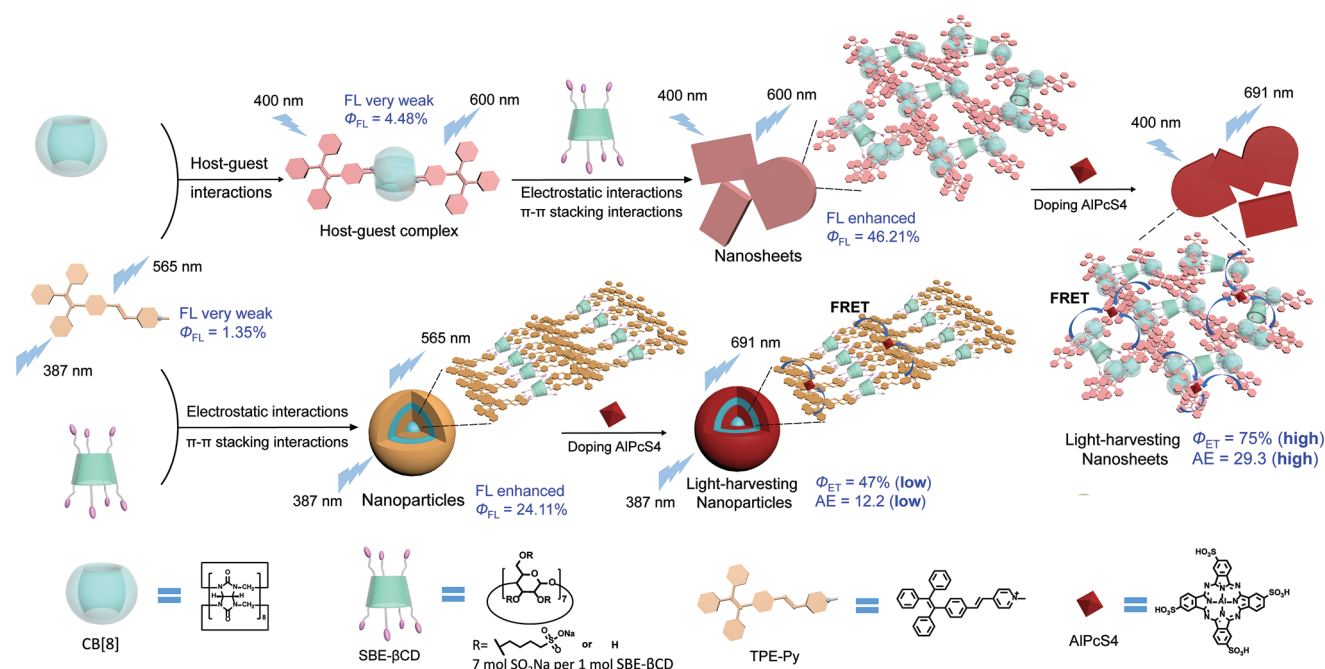
To achieve an efficient FRET process, two supramolecular macrocycles are introduced to facilitate the construction of multilevel assemblies. Among them, CB[8] was selected as the first macrocycles because the CB[8] can induce molecular dimerization,[14] molecular folding,[15] and molecular isomerization[16] through host–guest interactions,[17] thereby giving obviously luminescence change. Although the positively charged guests have been encapsulated by cucurbituril through host–guest interactions,[18] the exposed positively charged motif can also interact with the negatively charged macrocycles through the electrostatic interactions,[19] resulting in the enhancement of fluorescence intensity and change of the morphology, which was benefit to coassembly with dyes for an efficient FRET

M. Tian, H. Zhang
Faculty of Chemical Engineering
Kunming University of Science and Technology
Kunming, Yunnan 650500, P. R. China
E-mail: zhangheng0625@sina.com

Z. Wang, X. Yuan, Z. Liu, Y. Liu
College of Chemistry
State Key Laboratory of Elemento-Organic Chemistry
Nankai University
Tianjin 300071, P. R. China
E-mail: zhixue_liu@sina.com; yuliu@nankai.edu.cn

The ORCID identification number(s) for the author(s) of this article can be found under https://doi.org/10.1002/adfm.202300779.

**ADVANCED
SCIENCE NEWS**
www.advancedsciencenews.com

**ADVANCED
FUNCTIONAL
MATERIALS**
www.afm-journal.de

Scheme 1. Schematic illustration of the multilevel assembly mechanism of TPE-Py, CB[8], and SBE-*β*CD, as well as their FRET process with AlPcS4.

process. Especially in the light-harvesting energy transfer systems,[20] the introduction of electrostatic interactions is the most popular method to construct stable assemblies with low critical aggregation concentration.[21] Therefore, multiple charged cyclodextrins, which possess positively or negatively charged units on the primary and secondary side, were the best second candidate.[22] Meanwhile, the main component in cyclodextrins are D-glucose units rather than aromatic ring,[23] so the quenching phenomenon of fluorophore can also be avoided. Based on the successfully construction of the multilevel supramolecular assemblies through various noncovalent interactions, the modulation of topological morphology and multicolor luminescence behaviors will be realized.

Herein, we constructed multilevel supramolecular assemblies based on tetraphenylethylene pyridinium (TPE-Py), CB[8] and sulfobutylether-*β*-cyclodextrin (SBE-*β*CD) (**Scheme 1**). The first addition of CB[8] can form a 1:2 stoichiometric inclusion complex with TPE-Py through host–guest interactions with bathochromic shift about 35 nm. The second addition of negatively charged SBE-*β*CD coassembly with CB[8] complex to form nanosheets with enhanced fluorescence intensity through the electrostatic interactions. The formed ternary supramolecular assemblies TPE-Py⊂CB[8]@SBE-*β*CD served as excellent light-harvesting platform transferred the energy to the NIR dye sulfonated aluminum phthalocyanine (AlPcS4) with 75% energy transfer efficiency and an antenna effect of up to 29.3, accompanied by a bathochromic shift about 10 nm for AlPcS4 emission. By using multilevel supramolecular assemblies, it can be used for multicolor luminescence information storage and multiple logical gate systems.

Binding behavior between TPE-Py and CB[8] was first investigated by using the UV–vis absorption and fluorescence spectroscopy in aqueous solution. The TPE-Py possesses the maximum absorption peak at 387 nm, and then changed to 400 nm with the increase of CB[8] concentration (**Figure 1**a). Meanwhile, the fluorescence emission at 565 nm was also changed to 600 nm with addition of CB[8] (Figure 1b). Based on the strong bind interaction between positively charged TPE-Py and CB[8], the stoichiometry of the inclusion complex was calculated to be 1:2 of CB[8]:TPE-Py from a Job's plot (Figure S1a, Supporting Information). Therefore, the stepwise binding constants (*K*) can be calculated as 2.95×10^{11} M^{-2} by nonlinear least-squares fitting of the fluorescence titration between TPE-Py and CB[8] (Figure S1b, Supporting Information). In addition, the ^{1}H-NMR also confirmed the TPE-Py has a strong interaction with CB[8], with the chemical shift of pyridinium to the high field (Figure S2, Supporting Information).

To enhance the fluorescence intensity of TPE-Py⊂CB[8] inclusion complex, SBE-*β*CD was employed to coassembly because the negatively charged sulfonates can interact with TPE-Py through electrostatic interactions. As shown in Figure 1c, the fluorescence intensity at 600 nm enhanced obviously after adding the SBE-*β*CD, demonstrating that the SBE-*β*CD can be effectively coassembled with TPE-Py⊂CB[8], and fluorescence intensity was enhanced by a factor of 20 (Figure 1e). More content of SBE-*β*CD did not cause any fluorescence quenching or blue shift, demonstrating the stability of the coassembly TPE-Py⊂CB[8]@SBE-*β*CD. In order to investigate fluorescence enhancement, we compared the fluorescence behavior between TPE-Py and SBE-*β*CD. In the absence of CB[8], the SBE-*β*CD can also induce the tenfold fluorescence enhancement of TPE-Py, and continuing addition of SBE-*β*CD did not cause any fluorescence quenching, confirming that the electrostatic assembly of TPE-Py and SBE-*β*CD is the main effect of fluorescence enhancement, and the formed TPE-Py@SBE-*β*CD is also stable (Figure 1d,e). According to the excellent
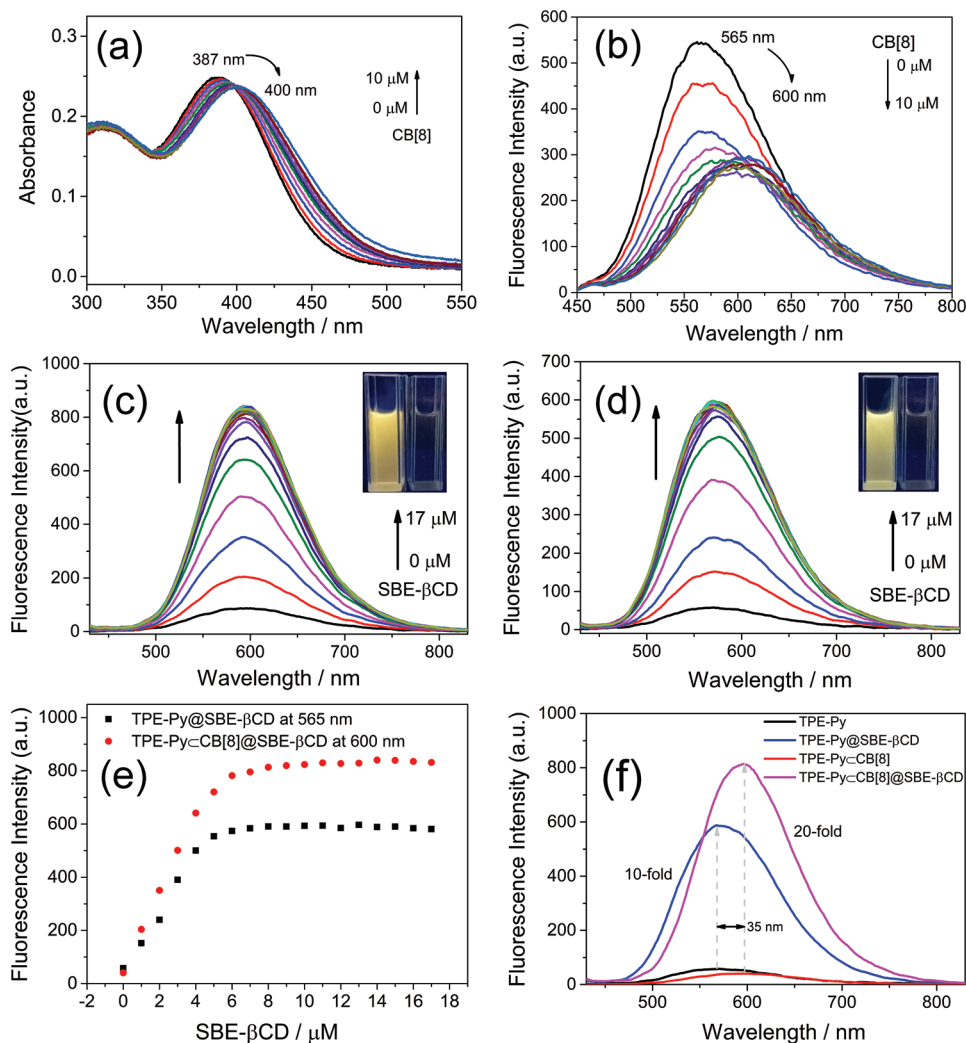
Figure 1. a) UV–vis absorption and b) fluorescence spectra of TPE-Py (10 µM) upon addition of CB[8] (0-10 µM) in aqueous solution (λ_{ex} = 400 nm; slits: 10/10 nm); Fluorescence spectra of c) TPE-Py⊂CB[8] and d) TPE-Py upon addition of SBE-βCD (0-17 µM) in aqueous solution (λ_{ex} = 400 nm; slits: 5/5 nm), Inset: Photographs of TPE-Py⊂CB[8] and TPE-Py upon addition of SBE-βCD under 365 nm irradiation. e) Fluorescence intensity of TPE-Py⊂CB[8] and TPE-Py upon addition of SBE-βCD. f) Fluorescence contrast analysis of TPE-Py, TPE-Py⊂CB[8], TPE-Py@SBE-βCD, TPE-Py⊂CB[8]@SBE-βCD.

fluorescence enhancement of the supramolecular assemblies in the presence of SBE-βCD, we compared the fluorescence spectra of TPE-Py, TPE-Py@SBE-βCD, TPE-Py⊂CB[8], and TPE-Py⊂CB[8]@SBE-βCD (Figure 1f). The TPE-Py displayed very weak fluorescence emission at 565 nm. Upon addition of SBE-βCD, the fluorescence intensity of TPE-Py can be increased tenfold without any bathochromic shift. While, upon addition of CB[8] in the TPE-Py solution, a bathochromic shift of 35 nm occurred in the fluorescence emission spectrum, displaying a weak fluorescence. Subsequently, after adding SBE-βCD in the solution of TPE-Py⊂CB[8], the fluorescence spectra occurred obviously enhanced without any blue shift. Meanwhile, the UV–vis spectra also showed that the addition of SBE-βCD did not change the TPE-Py⊂CB[8] absorption during the coassembly process (Figure S3, Supporting Information), confirming the stability of TPE-Py⊂CB[8]@SBE-βCD. The above results indicated that the first addition of CB[8] encapsulated TPE-Py through host–guest interactions, which respon-

sible for the bathochromic shift of the spectrum. The second addition of negatively charged SBE-βCD was in charge of fluorescence enhancement through the electrostatic interactions.

Subsequently, the assembly processes of SBE-βCD with TPE-Py and TPE-Py⊂CB[8] were measured at 600 nm optical transmittance. In the absence of SBE-βCD, the optical transmittance of TPE-Py was decreased gradually with the increase of concentration (**Figure 2**a; Figure S4a, Supporting Information). In contrast, the optical transmittance was decreased rapidly in the presence of SBE-βCD, and remains stable for concentrations greater than 35 µM (Figure 2b; Figure S4b, Supporting Information). The different optical transmittance changes demonstrated that the TPE-Py can self-aggregate by π–π stacking interactions, while the SBE-βCD can effectively induce the aggregation of TPE-Py and displayed a stable assembly through the π–π stacking interactions and electrostatic interactions, thereby significantly reduced critical aggregation concentration (CAC). A plot of optical transmittance at 600 nm versus TPE-Py
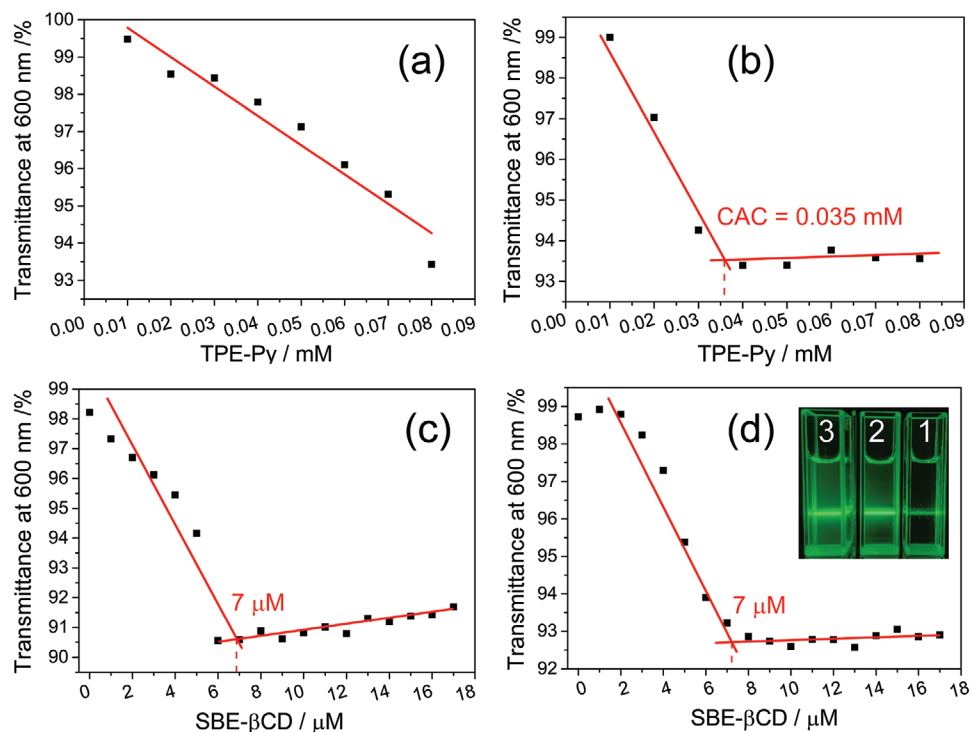
Figure 2. Optical transmittance changes of TPE-Py in the presence of SBE-βCD a) 0 μM and b) 5 μM; Optical transmittance changes of c) TPE-Py (40 μM) and d) TPE-Py⊂CB[8] (TPE-Py = 40 μM; CB[8] = 20 μM) with the different concentrations of SBE-βCD. Inset: Tyndall effects exhibited by 1) TPE-Py, 2) TPE-Py@SBE-βCD, 3) TPE-Py⊂CB[8]@SBE-βCD.

concentration demonstrated that the critical aggregation concentration was 35 μM in the presence of SBE-βCD. According to the calculation of CAC, the optimum molar ratio of TPE-Py@SBE-βCD and TPE-Py⊂CB[8]@SBE-βCD was evaluated on the concentration of TPE-Py at 40 μM. With the increase of SBE-βCD concentration, the optical transmittance decreased to a minimum of 91% and then increased slightly (Figure 2c; Figure S4c, Supporting Information), and the best mixing ratio for TPE-Py@SBE-βCD was calculated to be about 6:1. Similar, the minimum optical transmittance was also displayed at a TPE-Py⊂CB[8]@SBE-βCD molar ratio of about 6:1 and did not increase after further addition of SBE-βCD (Figure 2d; Figure S4d, Supporting Information), demonstrating the best mixing ratio was unchanged and the coassembly was very stable. Compared to the solutions of TPE-Py, a mixture solution of TPE-Py@SBE-βCD and TPE-Py⊂CB[8]@SBE-βCD at the ratio of 6:1 displayed a clear Tyndall effect (Figure 2d inset), demonstrating the formation of abundant supramolecular aggregates.

The assembly morphology of TPE-Py, TPE-Py@SBE-βCD, TPE-Py⊂CB[8], and TPE-Py⊂CB[8]@SBE-βCD were measured by transmission electron microscopy (TEM) (**Figure 3**). The TEM photos showed that the TPE-Py and TPE-Py⊂CB[8] complex were all formed irregular nanofragments. While, the TPE-Py@SBE-βCD gave obvious spherical nanoparticles with the diameters about 100 nm. In contrast, the assemblies of TPE-Py⊂CB[8]@SBE-βCD were shown as clear nanosheets with the diameters of about 500 nm. According to the morphologic transformation from nanoparticles of TPE-Py@SBE-βCD to nanosheets of TPE-Py⊂CB[8]@SBE-βCD, we confirmed

that the negatively charged SBE-βCD can interact with TPE-Py⊂CB[8] complex through electrostatic interactions. Meanwhile, the fluorescence quantum yields of TPE-Py and TPE-Py⊂CB[8] were measured to be 1.35% and 4.48%, respectively (Figure S5, Supporting Information). In contrast, the quantum yields of TPE-Py@SBE-βCD and TPE-Py⊂CB[8]@SBE-βCD displayed obvious enhanced as 24.11% and 46.21%, respectively. Because CB[8] has a strong binding affinity for TPE-Py, TPE-Py can be first encapsulated into the cavity of CB[8] through host–guest interactions, and then assembled with SBE-βCD through electrostatic interactions to form nanosheets, so as to obtain a high quantum yield of 46.21% due to the macrocycle confinement and secondary assembly. In contrast, the direct assembly of TPE-Py and SBE-βCD can form nanoparticles though only multiple electrostatic interactions, resulting in relatively low quantum yields of 24.11%. The lifetime of TPE-Py, TPE-Py⊂CB[8], TPE-Py@SBE-βCD, and TPE-Py⊂CB[8]@SBE-βCD were measured to be 1.88, 1.94, 4.11, 5.07 ns, respectively (Figure S6, Supporting Information). To investigate the mechanism of the assembly, we further evaluated the circular dichroism spectra of the assemblies. As shown in Figure S7 (Supporting Information), the spectra of TPE-Py@SBE-βCD and TPE-Py⊂CB[8]@SBE-βCD all displayed no Cotton effects, suggesting that the TPE-Py was not encapsulated in the SBE-βCD cavity. Therefore, the driving force for assembly was mainly dependent on the π–π stacking interactions of TPE-Py, CB[8] host–guest encapsulation, and electrostatic interactions.

By using the excellent fluorescence performance of the TPE-Py⊂CB[8]@SBE-βCD, it can be used as a good artificial light-harvesting platform for transferring the energy to a NIR dye, such
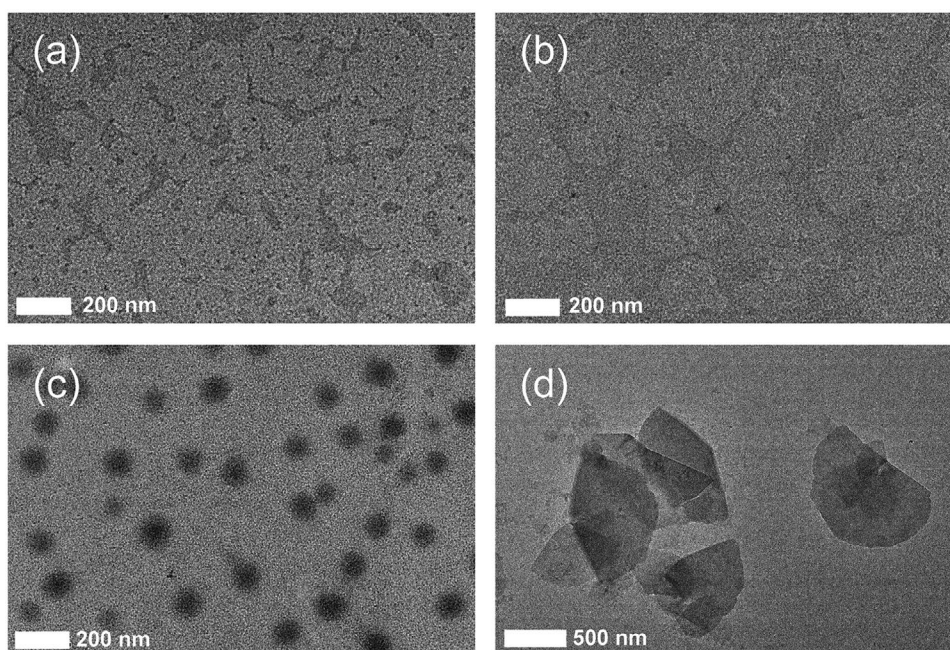
Figure 3. Transmission electron microscopy image of a) TPE-Py, b) TPE-Py⊂CB[8], c) TPE-Py@SBE-βCD, d) TPE-Py⊂CB[8]@SBE-βCD.

as sulfonated aluminum phthalocyanine (AlPcS4). After doping the AlPcS4 in the solution of the TPE-Py⊂CB[8]@SBE-βCD, the fluorescence intensity at 600 nm gradually decreased, accompanied by the enhancement of the fluorescence intensity at 693 nm (**Figure 4**a). According to the fluorescence quenching of the TPE-Py⊂CB[8]@SBE-βCD during the energy transfer process, the energy-transfer efficiency was calculated to be 75% (Figure S8a, Supporting Information), and the antenna effect was 29.3 at a donor/acceptor molar ratio of 278:1 (Figure 4b). In contrast, the TPE-Py@SBE-βCD also can transfer the energy to the AlPcS4 (Figure 4c). However, the fluorescence enhancement of the AlPcS4 was lower than that of the TPE-Py⊂CB[8]@SBE-βCD. The energy-transfer efficiency of TPE-Py@SBE-βCD to AlPcS4 was measured to be 47% and the antenna effect was only 12.2 (Figures S8b,c, Supporting Information). The reason of different energy-transfer efficiency and antenna effect may mainly be from the different overlaps between donor and acceptor. Because the TPE-Py⊂CB[8]@SBE-βCD displayed about 35 nm bathochromic shift of fluorescence emission more than TPE-Py@SBE-βCD due to the complexation of CB[8] and TPE-Py (Figure 4d), which increased the overlapped area with AlPcS4 absorption, thereby greatly enhanced the energy-transfer efficiency and antenna effect. Moreover, we found that the emission of AlPcS4 also occurred about a 10 nm bathochromic shift from 683 to 693 nm. The main reason may be that the doping of AlPcS4 into the supramolecular assembly can not only avoid the fluorescence quenching of the AlPcS4 self-aggregation, but also realized the fluorescence emission bathochromic shift through the assembly confinement. On the other hand, as compared to sulfato-β-cyclodextrin (SCD) without alkyl chains (Scheme S2, Supporting Information), SBE-βCD effectively improved its hydrophobicity, which was beneficial to the energy transfer process in multilevel supramolecular assemblies. The fluorescence titration experiments results displayed that SCD

can induce the fluorescence enhancement of TPE-Py and TPE-Py⊂CB[8] (Figure S9a,b, Supporting Information). However, no efficient energy transfer process occurs between TPE-Py@SCD and AlPcS4 (Figure S9c, Supporting Information), as well as between TPE-Py⊂CB[8]@SCD and AlPcS4 (Figure S9d, Supporting Information), confirming that the presence of SCD in such assemblies can only induce fluorescence enhancement and cannot construct efficient light-harvesting energy transfer systems.

To further investigate the light-harvesting process, we evaluated the quantum yields and fluorescence decay experiments. The quantum yields of TPE-Py@SBE-βCD@AlPcS4 and TPE-Py⊂CB[8]@SBE-βCD@AlPcS4 displayed obvious decreased as 12.20% and 11.13%, respectively (Figure S10, Supporting Information). The lifetime values of TPE-Py@SBE-βCD@AlPcS4 and TPE-Py⊂CB[8]@SBE-βCD@AlPcS4 were also decreased and measured to be 4.06 and 3.11 ns (Figure S11, Supporting Information), confirming the efficient energy transfer from the TPE-Py@SBE-βCD or TPE-Py⊂CB[8]@SBE-βCD to the AlPcS4 acceptor. In addition, the morphology of the TPE-Py@SBE-βCD@AlPcS4 and TPE-Py⊂CB[8]@SBE-βCD@AlPcS4 were further confirmed by using TEM (Figure S12, Supporting Information). After doping the AlPcS4 in the solution of TPE-Py@SBE-βCD and TPE-Py⊂CB[8]@SBE-βCD, there is no obvious morphology change during this energy transfer process. Based on the light-harvesting energy transfer process, we found that the supramolecular assembly strategy based on CB[8] and negatively charged cyclodextrin is beneficial to improve the energy transfer efficiency and antenna effect. Because the assemblies all have similar light yellow color, but the fluorescence is quite different, therefore can be used for the information storage. By using the different assembly solutions, the letters of N, K, U are indistinguishable under daylight, but can be interpreted under 365 nm irradiation (Figure 4e,f).
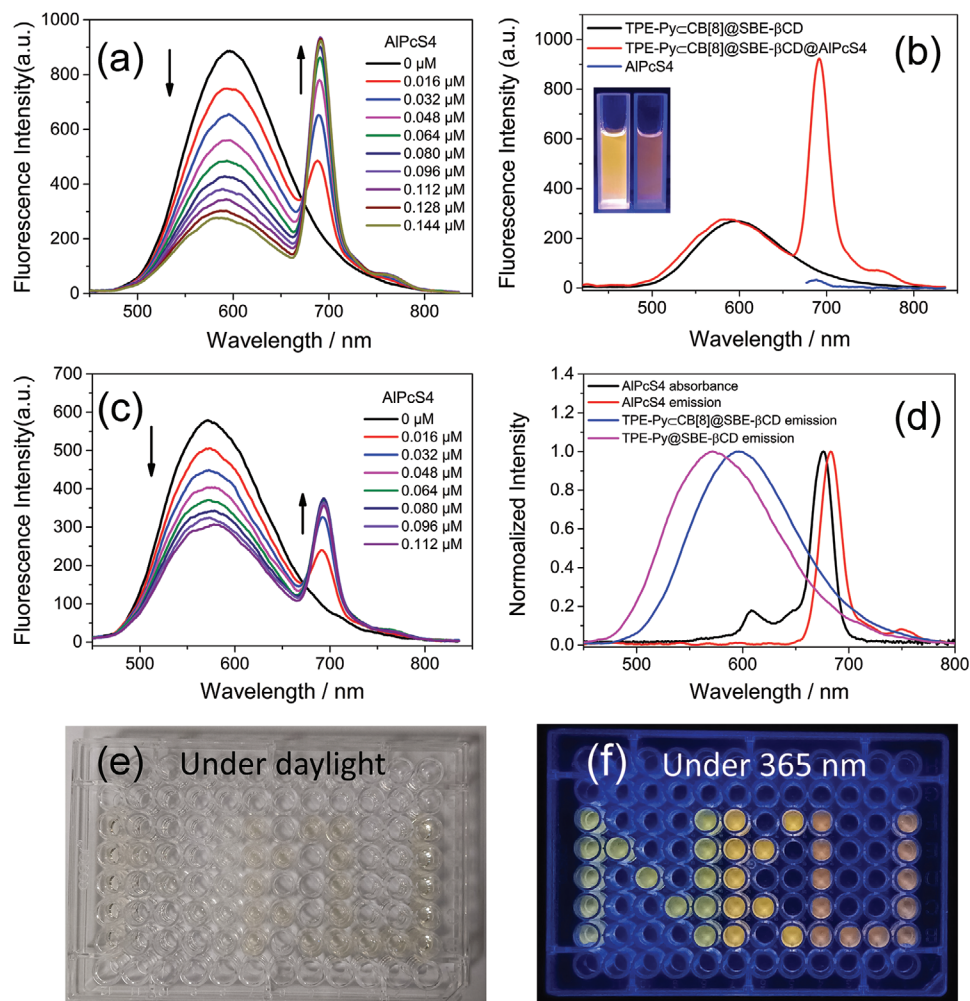
Figure 4. a) Fluorescence spectra of TPE-Py⊂CB[8]@SBE-βCD (TPE-Py = 40 μM, CB[8] = 20 μM, SBE-βCD = 8 μM) upon gradual addition of AlPcS4 (λ_{ex} = 400 nm; slits: 5/2.5 nm). b) Antenna effect maxima of TPE-Py⊂CB[8]@SBE-βCD@AlPcS4. (Red line: assemblies emission, λ_{ex} = 400 nm; blue line: AlPcS4 emission, λ_{ex} = 675 nm; black line: normalized emission spectrum of TPE-Py⊂CB[8]@SBE-βCD according to the red line. Inset: Photographs of TPE-Py⊂CB[8]@SBE-βCD and TPE-Py⊂CB[8]@SBE-βCD@AlPcS4 under 405 nm irradiation. c) Fluorescence spectra of TPE-Py@SBE-βCD (TPE-Py = 40 μM, SBE-βCD = 8 μM) upon gradual addition of AlPcS4 (λ_{ex} = 400 nm; slits: 5/2.5 nm). d) Normalized emission spectra of TPE-Py@SBE-βCD, TPE-Py⊂CB[8]@SBE-βCD and AlPcS4, as well as the normalized absorption spectrum of AlPcS4. e,f) Information storage of TPE-Py@SBE-βCD (N), TPE-Py⊂CB[8]@SBE-βCD (K), TPE-Py⊂CB[8]@SBE-βCD@AlPcS4 (U) under daylight and 365 nm irradiation.

With these satisfactory light-harvesting energy transfer process of multilevel supramolecular assemblies in mind, it can be used to construct multiple logic gate systems.[24] The logic device defined the different components of the assembly as inputs and the fluorescence emission intensity at 600 nm under excitation at 400 nm as output (**Figure 5**). For output, the fluorescence intensity above 750 is denoted as 1 and the one below as 0. Therefore, three INHIBIT logic gate systems with optical output were designed. Significantly, the output 0 and 1 states of the current logic circuit represent several different types of supramolecular assemblies. In three logical gate systems (Figure 5a–c), the fluorescence intensity at 600 nm can be "locked" in the coexistence of TPE-Py, CB[8], and SBE-βCD. AlPcS4 as a NOT gate was introduced, which can work in a platform with a "silent" signal output, and displayed clearly in the truth table (Figure 5d–f; Figure S13, Supporting Information). Although the simple logical gates were constructed by multilevel supramolecular assemblies, while the

increase of the inputs components made the output information becomes complicated, holding great potential for the construction of complex logic circuits.

2. Conclusion

In summary, we constructed an efficient light-harvesting supramolecular assembly based on TPE-Py, CB[8], SBE-βCD, and AlPcS4 through the host–guest interactions, π–π stacking interactions, and electrostatic interactions. In the assemblies, CB[8] encapsulated TPE-Py to form host-guest complexes with bathochromic shift about 35 nm, and then coassembly with SBE-βCD to form nanosheets with the enhancement of fluorescence intensity about 20 times through electrostatic interactions. The formed TPE-Py⊂CB[8]@SBE-βCD can be served as an excellent energy transfer platform to a NIR dye AlPcS4 with 75%

(a)

Input 1 TPE-Py⊂CB[8] @SBE-βCD	Input 2 AlPcS4	Output FL 600 nm
0	0	0
1	0	1
0	1	0
1	1	0

(b)

Input 1 TPE-Py@ SBE-βCD	Input 2 CB[8]	Input 3 AlPcS4	Output FL 600 nm
0	0	0	0
1	0	0	0
0	1	0	0
0	0	1	0
1	1	0	1
1	0	1	0
0	1	1	0
1	1	1	0

(c)

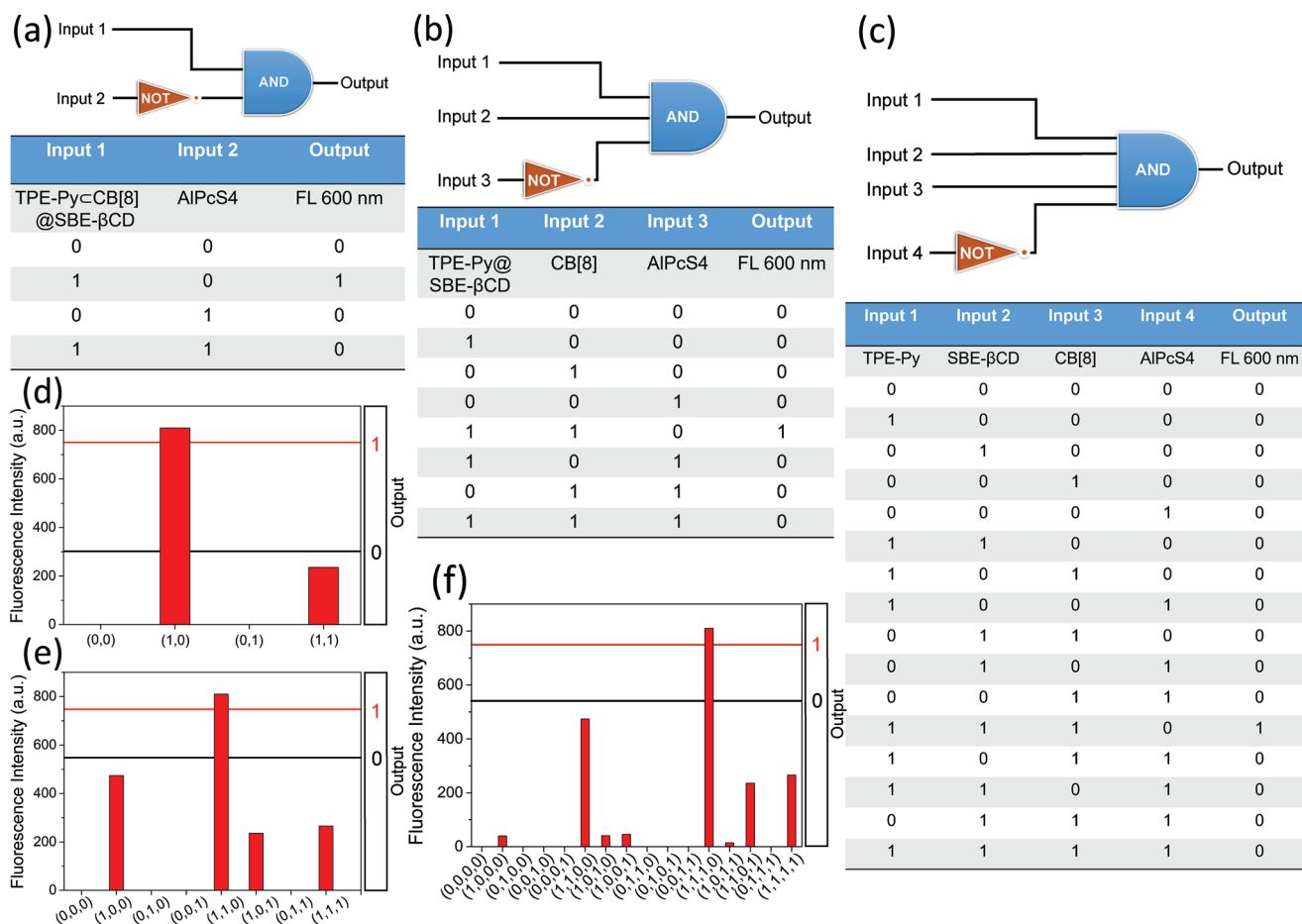| Input 1 TPE-Py	Input 2 SBE-βCD	Input 3 CB[8]	Input 4 AlPcS4	Output FL 600 nm
0	0	0	0	0
1	0	0	0	0
0	1	0	0	0
0	0	1	0	0
0	0	0	1	0
1	1	0	0	0
1	0	1	0	0
1	0	0	1	0
0	1	1	0	0
0	1	0	1	0
0	0	1	1	0
1	1	1	0	1
1	0	1	1	0
1	1	0	1	0
0	1	1	1	0
1	1	1	1	0

Figure 5. Scheme representation for a,b,c) three INHIBIT logic gates and d,e,f) the corresponding truth tables in the absence or presence of AlPcS4. The output is set to the intensity of fluorescence emission at 600 nm under excitation at 400 nm.

energy-transfer efficiency and an antenna effect value of 29.3, displaying clear NIR signal amplification with a bathochromic shift about 10 nm. The supramolecular coassembly strategy for making use of two kinds of macrocycles not only realized the bathochromic shift of emission spectra, but also enhanced their intensity. Benefiting from the multilevel supramolecular assemblies, multicolour luminescence information storage and multiple logical gate systems are successfully implemented.

Supporting Information

Supporting Information is available from the Wiley Online Library or from the author.

Conflict of Interest

The authors declare no conflict of interest.

Data Availability Statement

The data that support the findings of this study are available in the supplementary material of this article.

[1] a) L. Yang, X. Tan, Z. Wang, X. Zhang, *Chem. Rev.* **2015**, *115*, 7196; b) Q. Song, S. Goia, J. Yang, S. C. L. Hall, M. Staniforth, V. G. Stavros, S. Perrier, *J. Am. Chem. Soc.* **2021**, *143*, 382; c) P. Xing, Y. Zhao, *Acc. Chem. Res.* **2018**, *51*, 2324.

[2] Y. Xu, A. Hao, P. Xing, *Angew. Chem., Int. Ed.* **2022**, *61*, 202113786.

[3] a) B. Hua, L. Shao, M. Li, H. Liang, F. Huang, *Acc. Chem. Res.* **2022**, *55*, 1025; b) Y. Liu, H. Yang, Z. Wang, X. Zhang, *Chem Asian J* **2013**, *8*, 1626.

[4] a) H. J. Yu, X. L. Zhou, X. Dai, F. F. Shen, Q. Zhou, Y. M. Zhang, X. Xu, Y. Liu, *Chem. Sci.* **2022**, *13*, 8187; b) Y. Liu, Z. Huang, X. Tan, Z. Wang, X. Zhang, *Chem. Commun.* **2013**, *49*, 5766; c) J. D. Barrio, J. Liu, R. A. Brady, C. S. Y. Tan, S. Chiodini, M. Ricci, R. Fernandez-Leiro, C. J. Tsai, P. Vasileiadi, L. Di Michele, D. Lairez, C. Toprakcioglu, O. A. Scherman, *J. Am. Chem. Soc.* **2019**, *141*, 14021.

[5] a) Z. Liu, Y. Liu, *Chem. Soc. Rev.* **2022**, *51*, 4786; b) Z. Yu, F. Tantakitti, T. Yu, L. C. Palmer, G. C. Schatz, S. I. Stupp, *Science* **2016**, *351*, 497.

[6] a) C. Tu, W. Wu, W. Liang, D. Zhang, W. Xu, S. Wan, W. Lu, C. Yang, *Angew. Chem., Int. Ed.* **2022**, *61*, 202203541; b) X. Song, X. Zhu, S. Qiu, W. Tian, M. Liu, *Angew. Chem., Int. Ed.* **2022**, *61*, 202208574; c) D. L. Wang, J. Y. Gong, Y. Xiong, H. Z. Wu, Z. Zhao, D. Wang, B. Z. Tang, *Adv. Funct. Mater.* **2022**, *33*, 2208895; d) X. H. Chen, Y. X. Li, S. W. Li, M. Gao, L. Ren, B. Z. Tang, *Adv. Funct. Mater.* **2018**, *28*, 1804362; e) P. Xing, C. Yang, Y. Wang, S. Z. F. Phua, Y. Zhao, *Adv. Funct. Mater.* **2018**, *28*, 1802859.

[7] a) Z. Yu, H. K. Bisoyi, X. M. Chen, Z. Z. Nie, M. Wang, H. Yang, Q. Li, *Angew. Chem., Int. Ed.* **2022**, *61*, 202200466; b) G. Wu, Z. Huang, O. A. Scherman, *Angew. Chem., Int. Ed.* **2020**, *59*, 15963.

[8] a) Y. Mei, Q. W. Zhang, Q. Gu, Z. Liu, X. He, Y. Tian, *J. Am. Chem. Soc.* **2022**, *144*, 2351; b) J. H. Tian, X. Y. Hu, Z. Y. Hu, H. W. Tian, J. J. Li, Y. C. Pan, H. B. Li, D. S. Guo, *Nat. Commun.* **2022**, *13*, 4293.

[9] a) Y. Zhao, S. Song, X. Ren, J. Zhang, Q. Lin, Y. Zhao, *Chem. Rev.* **2022**, *122*, 5604; b) G. Sinawang, M. Osaki, Y. Takashima, H. Yamaguchi, A. Harada, *Chem. Commun.* **2020**, *56*, 4381.

[10] X. Chen, H. K. Bisoyi, X.-F. Chen, X.-M. Chen, S. Zhang, Y. Tang, G. Zhu, H. Yang, Q. Li, *Matter* **2022**, *5*, 3883.

[11] S. Garain, B. C. Garain, M. Eswaramoorthy, S. K. Pati, S. J. George, *Angew. Chem., Int. Ed.* **2021**, *60*, 19720.

[12] X. Y. Dai, M. Huo, X. Dong, Y. Y. Hu, Y. Liu, *Adv. Mater.* **2022**, *34*, 2203534.

[13] X. M. Chen, Y. Chen, Q. Yu, B. H. Gu, Y. Liu, *Angew. Chem., Int. Ed.* **2018**, *57*, 12519.

[14] G. Wu, F. Li, B. Tang, X. Zhang, *J. Am. Chem. Soc.* **2022**, *144*, 14962.

[15] X. K. Ma, W. Zhang, Z. Liu, H. Zhang, B. Zhang, Y. Liu, *Adv. Mater.* **2021**, *33*, 2007476.

[16] X. Sun, Z. Liu, Z. Wang, M. Huo, H. Y. Zhang, Y. Liu, *J. Org. Chem.* **2022**, *87*, 7658.

[17] H. Nie, Z. Wei, X. L. Ni, Y. Liu, *Chem. Rev.* **2022**, *122*, 9032.

[18] a) S. Mommer, K. Sokolowski, M. Olesinska, Z. Huang, O. A. Scherman, *Chem. Sci.* **2022**, *13*, 8791; b) B. Xiao, S. He, M. Sun, J. Zhou, Z. Wang, Y. Li, S. Liu, W. M. Nau, S. Chang, *Angew. Chem., Int. Ed.* **2022**, *61*, 202203830; c) L. L. Tan, M. Wei, L. Shang, Y. W. Yang, *Adv. Funct. Mater.* **2020**, *31*, 2007277.

[19] Z. Liu, X. Dai, Y. Sun, Y. Liu, *Aggregate* **2020**, *1*, 31.

[20] a) Z. Liu, X. Sun, X. Dai, J. Li, P. Li, Y. Liu, *J. Mater. Chem. C* **2021**, *9*, 1958; b) L. Xu, Z. Wang, R. Wang, L. Wang, X. He, H. Jiang, H. Tang, D. Cao, B. Z. Tang, *Angew. Chem., Int. Ed.* **2020**, *59*, 9908; c) W. J. Li, X. Q. Wang, D. Y. Zhang, Y. X. Hu, W. T. Xu, L. Xu, W. Wang, H. B. Yang, *Angew. Chem., Int. Ed.* **2021**, *60*, 18761.

[21] a) X. M. Chen, Q. Cao, H. K. Bisoyi, M. Wang, H. Yang, Q. Li, *Angew. Chem., Int. Ed.* **2020**, *59*, 10493; b) S. Guo, Y. Song, Y. He, X. Y. Hu, L. Wang, *Angew. Chem., Int. Ed.* **2018**, *57*, 3163; c) K. Wang, K. Velmurugan, B. Li, X. Y. Hu, *Chem. Commun.* **2021**, *57*, 13641.

[22] a) J. J. Li, Y. Chen, J. Yu, N. Cheng, Y. Liu, *Adv. Mater.* **2017**, *29*, 1701905; b) Z. Liu, W. Lin, Y. Liu, *Acc. Chem. Res.* **2022**, *55*, 3417.

[23] a) Z. Liu, M. Tian, H. Zhang, Y. Liu, *Chem. Commun.* **2023**, *59*, 896; b) Z. Liu, X. Dai, Q. Xu, X. Sun, Y. Liu, *Chin. J. Chem.* **2022**, *40*, 493; c) G. M. Russell, T. Kaneko, S. Ishino, H. Masai, J. Terao, *Adv. Funct. Mater.* **2022**, *32*, 2205855.

[24] a) J. Cao, X. Ma, M. Min, T. Cao, S. Wu, H. Tian, *Chem. Commun.* **2014**, *50*, 3224; b) H. Li, J. N. Zhang, W. Zhou, H. Zhang, Q. Zhang, D. H. Qu, H. Tian, *Org. Lett.* **2013**, *15*, 3070; c) X. Zhou, X. Wu, J. Yoon, *Chem. Commun.* **2015**, *51*, 111.